Triggering mechanism and tsunamogenic potential of the Cape Fear Slide complex, U.S. Atlantic margin

Matthew J. Hornbach and Luc L. Lavier

Institute for Geophysics, University of Texas, 4412 Spicewood Springs Road, Building 600, Austin, Texas 78759, USA (matth@ig.utexas.edu)

Carolyn D. Ruppel

U.S. Geological Survey, 384 Woods Hole Road, Woods Hole, Massachusetts 02543, USA

[1] Analysis of new multibeam bathymetry data and seismic Chirp data acquired over the Cape Fear Slide complex on the U.S. Atlantic margin suggests that at least 5 major submarine slides have likely occurred there within the past 30,000 years, indicating that repetitive, large-scale mass wasting and associated tsunamis may be more common in this area than previously believed. Gas hydrate deposits and associated free gas as well as salt tectonics have been implicated in previous studies as triggers for the major Cape Fear slide events. Analysis of the interaction of the gas hydrate phase boundary and the various generations of slides indicates that only the most landward slide likely intersected the phase boundary and inferred high gas pressures below it. For much of the region, we believe that displacement along a newly recognized normal fault led to upward migration of salt, oversteepening of slopes, and repeated slope failures. Using new constraints on slide morphology, we develop the first tsunami model for the Cape Fear Slide complex. Our results indicate that if the most seaward Cape Fear slide event occurred today, it could produce waves in excess of 2 m at the present-day 100 m bathymetric contour.

1. Introduction

[2] Submarine slides are ubiquitous along the North American Atlantic continental slope, yet the frequency of these slide occurrences remains poorly constrained. Since 40 ka, at least 10 major (>100 km³) mass wasting events have been documented in the North Atlantic [*Maslin et al.*, 2004].

Some of these mass movements, such as the 1929 Grand Banks Slide (~185 km³), have occurred in historic times and have been well-documented [*Heezen and Ewing*, 1952; *Maslin et al.*, 2004; *Piper and Asku*, 1987].

[3] The triggering mechanisms for larger slides remain controversial [*Driscoll et al.*, 2000; *Embley*,

1980; *Maslin et al.*, 2004, 2005; *O'Leary and Dobson*, 1992; *Paull et al.*, 1996a; *Popenoe et al.*, 1993]. Potential triggers that may act alone or in consort include earthquakes, mechanical failure of overpressured sediments, storm waves, groundwater seepage, failure of oversteepened slopes, gas hydrate dissociation, and sea level change [*Bea et al.*, 1983; *Dugan and Flemings*, 2000; *Hampton et al.*, 1996; *Kayen and Lee*, 1993; *Locat and Lee*, 2002; *Mienert et al.*, 2005; *Paull et al.*, 1996a; *Schmuck and Paull*, 1993; *Solheim et al.*, 2005; *Sultan et al.*, 2004a, 2004b]. The interaction among slope failures, sea level change, and gas hydrate and free gas deposits in continental margin sediments has been a research direction with significant interest owing to the implications for large scale methane releases to the ocean and atmosphere and for climate change [*Maslin et al.*, 1998, 2004; *Paull et al.*, 2003; *Pecher et al.*, 2005; *Vanneste et al.*, 2006].

[4] The rapid displacement of large volumes of material during some submarine slide events can also lead to tsunami generation. For most of the North American Atlantic margin, though, no thorough assessment of the tsunamogenic potential of past or possible future slide events has been undertaken. With the rapid increase in worldwide coastal populations over the past 50 years, developing an understanding of tsunami generation by offshore submarine slides has significant societal relevance.

[5] In this paper, we focus on the evolution, triggers, and tsunamogenic potential of the Cape Fear Slide, one of the largest submarine slides (~25,000 km^2) on the U.S. Atlantic Coast [*Embley*, 1980]. Although large, the size of the Cape Fear Slide complex is by no means unusual, since several other comparable or perhaps even larger mass wasting events have been documented across the Western North Atlantic Margin [*Booth et al.*, 1993; *Embley and Jacobi*, 1986]. Using recently acquired geophysical data, we first refine the history of slides in the Cape Fear region. We then combine the new geologic interpretation with older data to assess possible trigger mechanisms at the site. Finally, we develop preliminary tsunami scenarios for past slides in the Cape Fear area.

2. Geologic Setting and Previous Interpretations

[6] The Cape Fear Slide (CFS) complex is located ~200 km southeast of Cape Fear, North Carolina

on the eastern, seaward-facing side of the Carolina Trough, a long, narrow, Triassic-Jurassic rift basin that strikes NNE along the continental slope (roughly outboard of ~1000 m water depth) from Charleston to Cape Hatteras (Figure 1). The Carolina Trough contains more than 6 km of compacted, post-rift sediments and likely formed via post-rift tectonism and salt mobilization [*Dillon et al.*, 1982; *Dillon and Popenoe*, 1988]. *Dillon et al.* [1982] postulate that salt migrated both seaward and upward during Jurassic time, producing subsidence where salt had been withdrawn. The trough is flanked on the west by a large growth fault and on the east by a linear chain of ~25 diapirs that approach and even breach the seafloor [*Dillon et al.*, 1982].

[7] Within the CFS complex, previous studies have identified three slide headwalls on the eastern edge of the Carolina Trough. The CFS slides are associated with archetypal headwall crown scarps, identified by scallop-shaped semi-circular escarpments facing down slope [*Carpenter*, 1981; *Crozier*, 1984; *Hampton et al.*, 1996; *Popenoe et al.*, 1993]. The crown-shaped headwall for the main CFS scarp lies ~2300 m below sea level (mbsl), is ~50 km long, as much as 120 m high, and has a sediment apron extending more than 300 km downslope [*Cashman and Popenoe*, 1985; *Embley*, 1980; *Popenoe et al.*, 1993]. High-resolution side-scan sonar images of this headwall reveal a continuous scarp with slide tracks, debris fields, and exposed bedding [*Cashman and Popenoe*, 1985]. The uppermost CFS headwall, located at ~890 mbsl, also has a crown-shape morphology and is ~10 km long and 20 m high [*Carpenter*, 1981]. GLORIA side-scan sonar images show that the main part of the CFS was a large event, with debris from the slide covering perhaps 5,000–36,000 km^2 [*Cashman and Popenoe*, 1985; *Dillon and Popenoe*, 1988; *Embley*, 1980; *Popenoe et al.*, 1993; *Scanlon*, 1982; *ten Brink et al.*, 2007]. Geochronologic studies of sediment associated with mass-wasting at the CFS indicate at least two mass-wasting events during the last sea level low-stand from ~28 ka to ~13 ka [*Paull et al.*, 1996a; *Rodriguez and Paull*, 2000].

[8] Two key explanations have been advanced to describe the formation of the CFS complex, and both remain untested. *Carpenter* [1981], who first recognized the occurrence of a gas hydrate phase boundary beneath the uppermost CFS, suggested that free gas, possibly produced by gas hydrate dissociation, may have increased subsurface fluid
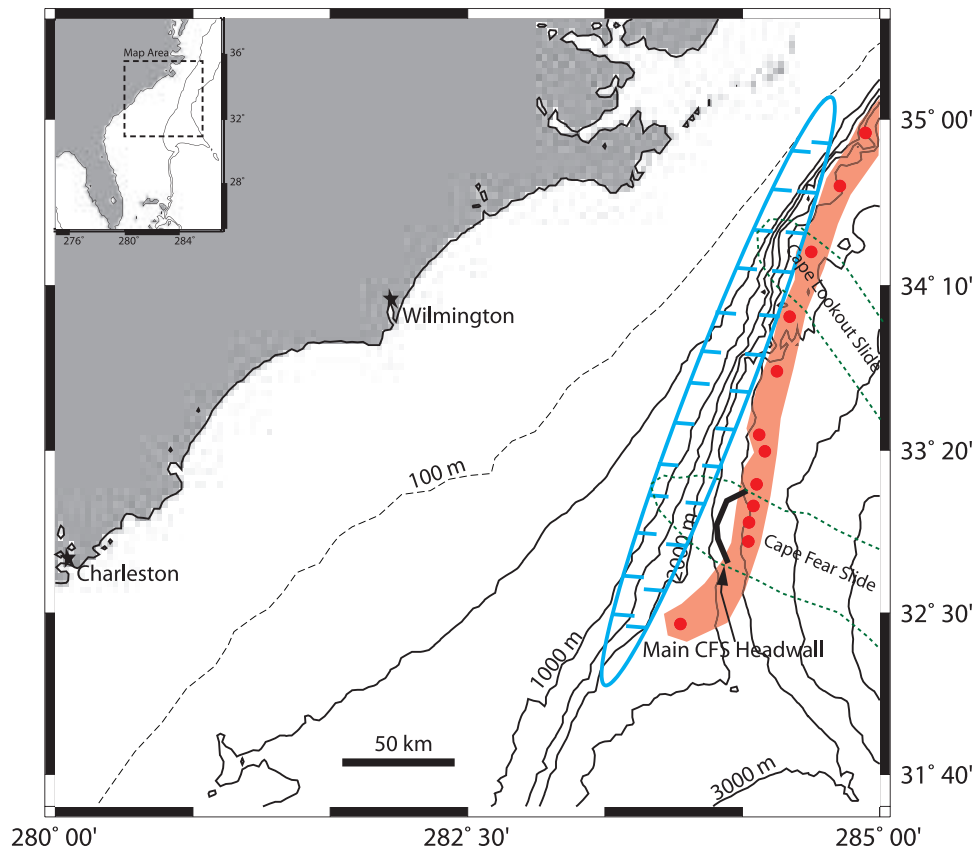
Figure 1. Map after *Dillon et al.* [1982], showing the general location of the main CFS headwall and debris field, the Carolina Trough outlined in blue, and the approximate location of a linear chain of salt diapirs, denoted as red circles. Contour interval is 500 m, with the exception of the 100 m contour.

pressures, reduced sediment cohesion, and ultimately triggered sliding. Likewise, *Popenoe et al.* [1993] and *Schmuck and Paull* [1993] inferred the presence of significant methane hydrate and free gas deposits beneath the lower CFS, leading to a similar hypothesis that sea level lowering or bottom water temperature changes may have dissociated hydrate, released gas, and reduced sediment cohesion in the region [*Driscoll et al.*, 2000; *Paull et al.*, 1996a; *Popenoe et al.*, 1993; *Schmuck and Paull*, 1993].

[9] Just east of the main CFS headwall, three salt diapirs lie within the slide debris field. An alternative explanation for CFS formation is triggering by displacement along faults that formed to accommodate regional salt intrusion near the main CFS headwall [*Popenoe et al.*, 1993]. In this scenario, salt intrusion causes slope steepening that initially triggers sliding. Subsequent slide episodes stem from progressive upslope failure along seaward-dipping listric faults as downslope support for the upslope sediments is removed [*Cashman and*

Popenoe, 1985; *Dillon et al.*, 1982]. *Cashman and Popenoe* [1985] also suggest that the main CFS scarp likely formed along preexisting faults and fault crown cracks created by salt intrusion [*Hampton et al.*, 1996].

3. Data Collection and Processing

[10] The new data used for this study were collected on the R/V *Atlantis* in July 2003. Multibeam swath bathymetric data were acquired with the *Atlantis*'s hull-mounted SeaBeam 2100/12 system. These data were merged, converted into grid files using MB-System software [*Caress and Chayes*, 1995] and visually displayed using Generic Mapping Tool (GMT) software [*Wessel and Smith*, 1991].

[11] We also collected single channel Chirp data using a Knudsen 320B/R echosounder with hull-mounted transducers. The echosounder emitted a sweeping signal from 1.5–11.5 kHz with a Chirp rate that varied directly with water depth. Raw data

were saved in SEGY format, deconvolved and filtered using SIOSEIS software [*Henkart*, 2006], and interpreted using Paradigm Geophysical software.

4. Results

4.1. New Constraints on Slide Morphology and Chronology

[12] The newly acquired data were used to produce high-resolution multibeam bathymetric images encompassing both the upper and lower headwalls of the CFS complex. The bathymetric images, combined with Chirp data, allow detailed interpretation of seafloor features, shallow structure, and the relationship among multiple slide events. The multibeam image (Figure 2) reveals at least 5 major escarpments (labeled S1 through S5) exposed at the seafloor and perhaps others buried within the CFS complex. The headwall of each distinct slide is clearly visible in bathymetric data and on Chirp profiles. The data show little, if any, evidence for sediment onlap, suggesting that most of these slide events happened relatively recently (Figures 2, 3, and 4). Carbon-14 dating of sediments shows a gap in age between 14 ka and 30 ka in material recovered from the lower slide, which is associated with the S4 scarp; this slide event occurred during the last sea level lowstand [*Paull et al.*, 1996a; *Rodriguez and Paull*, 2000]. Discontinuous age profiles were also observed in cores located above the main CFS, with some of these ages indicating slope failure within the same time frame [*Paull et al.*, 1996a; *Rodriguez and Paull*, 2000].

[13] The most westwardly and shallowest (∼890 mbsl) scarp (S1) has a crown-shaped headwall that extends downslope for at least 40 km on both sides of the slide scar (Figures 2 and 3). Downslope, this S1 scarp crosscuts other scarps, including the highest headwall scarp (S4), which is part of the main CFS complex (S4 and S5). Within the S1 debris field but upslope of the main headwall (S4–S5 headwalls) are two additional scarps S2 and S3 (Figures 2 and 3). The S2 scarp is a ∼20 km long and ∼3 km wide chute that widens abruptly downslope. Chirp line 30 shows a headwall height of at least 30 m for S2, as well as evidence for an older, buried headwall directly south of the S2 slide event (Figure 4a). There is also evidence for a younger slide (S3) that disrupts the S2 scarp. The S3 scarp, which is associated with the smallest disrupted area, overlaps the S2 scarp and has an
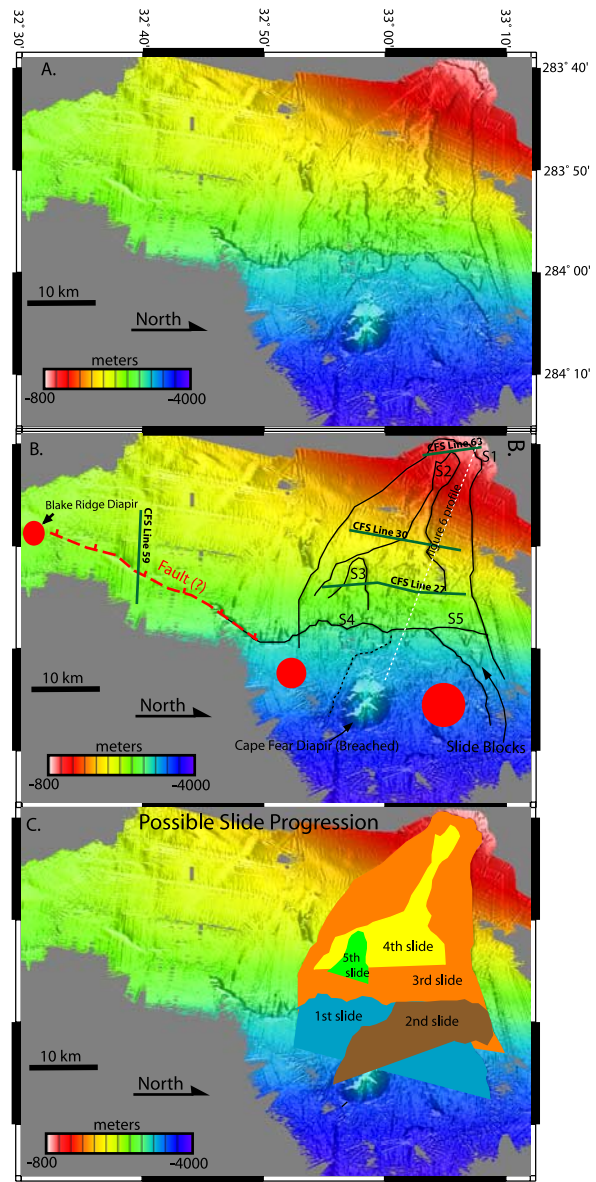
Figure 2. New multibeam data of the Cape Fear Slide complex, with ∼100 m lateral resolution. (a) Data with no interpretation. (b) Location of S1 to S5 scarps, inferred subsurface salt diapirs (red circles), the breached Cape Fear Diapir, the newly inferred normal fault, and the profile shown in Figure 5 (dashed white line). (c) A proposed scenario for relative slide timing based on the overlap and location of different slide headwalls.

escarpment height of at least 20 m above the rupture surface (Figure 4b).

[14] The main CFS headwall (S4), also a crown-shaped escarpment, is perhaps the largest slide in the complex. The S4 scarp has a ∼120 m high headwall that extends ∼50 km from north to south.
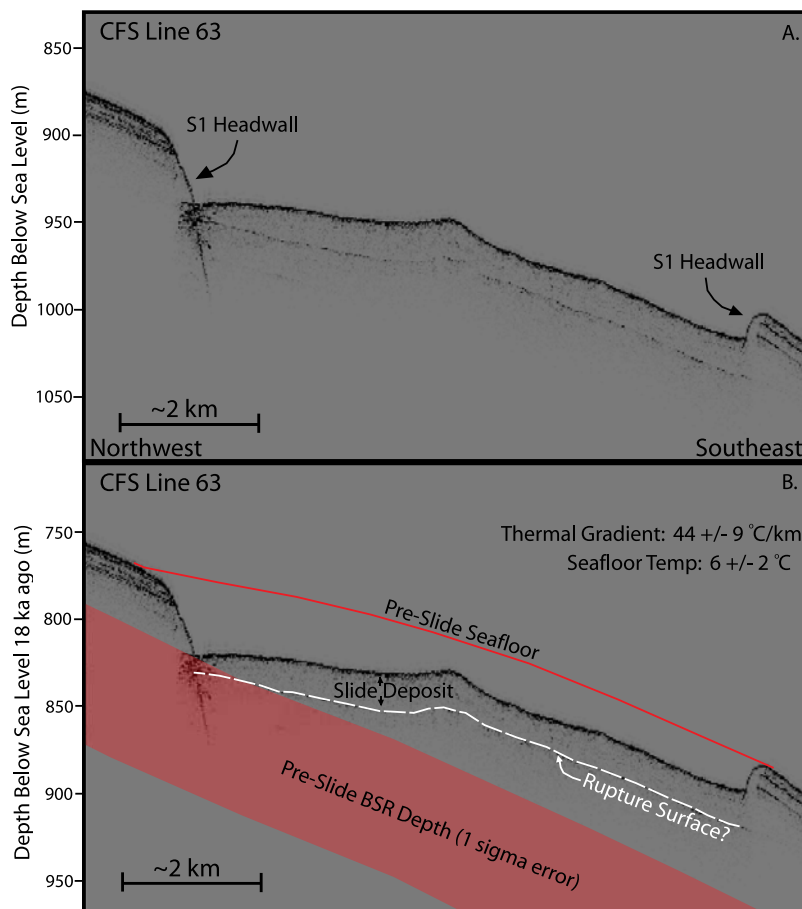
Figure 3. (a) Uninterpreted and (b) interpreted image of CFS Chirp line 63, which obliquely crosses the uppermost S1 slide headwall. The interpreted section shows the predicted depth of the gas hydrate phase boundary during the last sea level lowstand. Note that the slide rupture surface is predicted to cross the phase boundary on the northwest side of the profile. The rupture surface reflection only occurs below the slide feature, not outside the slide, and no other continuous or coherent reflection exists within the slide debris field.

The extreme southern end of the S4 escarpment follows an upslope path that converges with a previously unidentified north-south linear depression running subparallel to the continental slope break (Figure 2). Analysis of regional Chirp line 59, which was acquired across this depression, suggests that this ~40-km-long feature represents the scarp of a previously unrecognized, seafloor-breaching normal fault that is discussed in greater detail below (Figure 5).

[15] The northern flank of the main S4 scarp is intersected by the S5 scarp, which represents a secondary slide. The S5 scarp extends at least 10 km north of the main S4 slide, with a headwall height of at least 30 m. On bathymetric data, kilometer-wide slide blocks can be clearly discerned seaward of the S5 headwall (Figure 2).

4.2. Triggering Mechanisms for the Cape Fear Slide Events

4.2.1. Methane Hydrate and Free Gas

[16] Previous studies [*Carpenter*, 1981; *Schmuck and Paull*, 1993] suggest the present-day occurrence of methane hydrate and accumulations of free gas in the sediments of the CFS region, leading to the hypothesis that gas overpressures may have played a role in past slope failures. Regional Chirp lines reveal distinct, shallow (<40 m below the seafloor), apparent unconformities below several of the CFS rubble fields (Figure 4). We detect clear, continuous reflectors beneath some of the apparent unconformities (Figure 4b). The reflectors that lie below the unconformities generally occur where the seafloor is
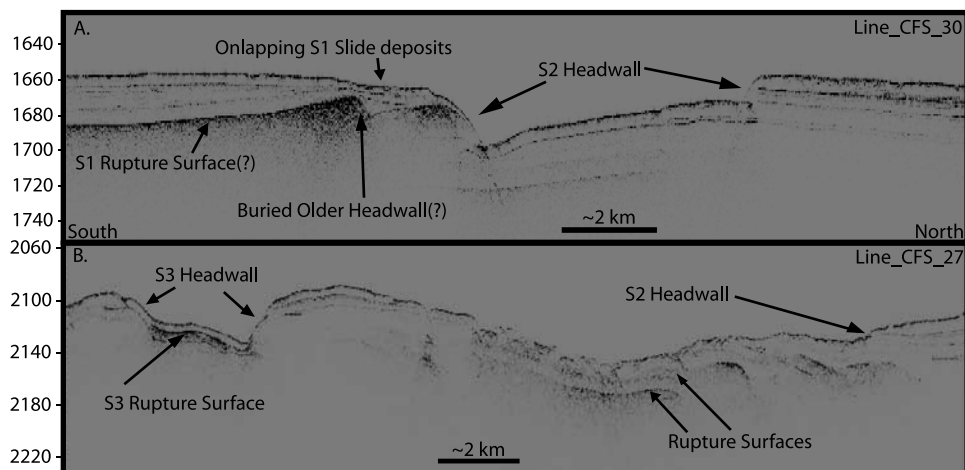
Figure 4. Interpreted Chirp lines (a) 30 and (b) 27, which cross through the middle of the CFS complex. (a) Line 30 shows a high-amplitude unconformity that we interpret as the S1 rupture surface. A depth offset in this unconformity appears surprisingly similar to the offset observed at exposed seafloor headwalls, and this unconformity may represent an older buried slide event. The S2 headwall is also clearly visible. (b) High-amplitude unconformities in Chirp Line 27 are similar to those in Line 30, but some of the unconformities (e.g., below the S3 slide) appear layered, perhaps indicating multiple, separate rupture surfaces associated with distinct slide events at the site.
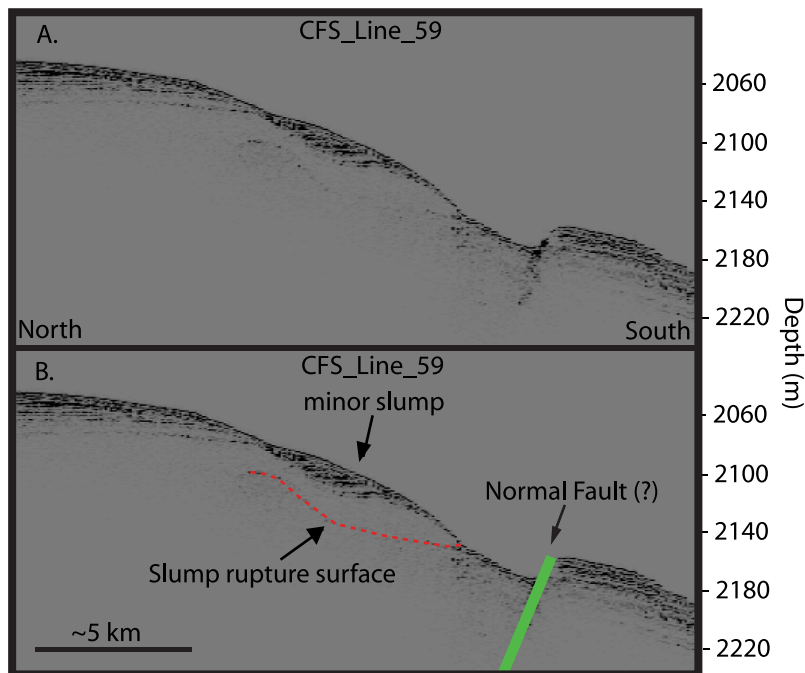
Figure 5. An (a) uninterpreted and (b) interpreted section of Chirp line 59, located between the Blake Ridge Diapir and Cape Fear Diapir. An ENE-dipping normal fault cuts through the profile, and the scarp is exposed at the seafloor. The slump in the hanging wall of the normal fault may have been caused by steepening of the slope in response to downward displacement of the slope.

relatively flat-lying, and no significant out-of-plane reflections are expected. Thus these subunconformity events are likely real, in-plane reflections.

[17] We submit that these unconformities represent slide rupture surfaces and not concentrated hydrate or free gas. We can eliminate free gas as the source of the reflector by calculating the depth of hydrate stability zone in the region. Using the CSMHYD gas hydrate stability code provided by *Sloan* [1998], we calculate the stability field for pure methane hydrate in equilibrium with pore water having 3.3‰ salt. In this passive margin setting, methane is by far the most common hydrate former, and the assumption of standard seawater salinity is a valuable first step in estimating in situ stability conditions. Based on the known water depth, assumed bottom water temperature [*Roemmich and Wunsch*, 1985], and thermal gradient data acquired within the CFS area [*Ruppel et al.*, 1995], we predict that methane hydrate, not free gas, is the stable phase at the depths of the unconformities. Therefore we infer that these anomalous reflectors are most likely buried slide rupture surfaces (i.e., the scarps associated with previous mass wasting events) or possibly carbonate-rich horizons or internal reflectors within gas hydrate-bearing sediments. At many locations, *Hampton et al.* [1996] document anomalously strong reflectors beneath slide deposits in Chirp data and interpret these as ancient slide rupture surfaces. At the CFS, the disappearance of these unconformities outside of slide zones (Figures 3 and 4) strongly argues for a genetic relationship between these features and mass wasting events.

[18] The inference that seismic reflectors may merely represent slide rupture surfaces does not preclude gas hydrate or free gas from having played a role in triggering one or more CFS events. Elevated pore pressures, which can trigger slides by lowering the threshold for the mechanical failure sediments, may arise at the base of gas hydrate stability [*Flemings et al.*, 2003; *Hornbach et al.*, 2004; *Kayen and Lee*, 1993], and strong bottom simulating reflectors (BSR) that mark the base of gas hydrate stability are observed throughout the present-day CFS [*Carpenter*, 1981; *Popenoe et al.*, 1993].

[19] Although the gas hydrate phase boundary is currently tens to hundreds of meters below most CFS rupture surfaces [*Carpenter*, 1981; *Popenoe et al.*, 1993], sea level was as much as 120 m lower during the last sea level lowstand, when the CFS complex most likely developed [*Maslin et al.*,

2004; *Paull et al.*, 1996a]. For the present-day case, we estimate that the base of gas hydrate stability lies at 134±40 m at the shallowest (~890 mbsl) part of the upper (S1) CFS headwall if we assume bottom water temperature of $6.0 \pm 2.0°C$, thermal gradient of $44 \pm 9°C$ km^{-1} [*Ruppel et al.*, 1995], 3.3‰ NaCl pore water, and methane as the only hydrate former. This predicted depth is consistent with the depth of high-amplitude, seismic bright spots discussed by [*Carpenter*, 1981]. At 18 ka, BSR depth would have been 98 ± 40 m below seafloor assuming the same parameters, but bottom water that was slightly warmer [*Roemmich and Wunsch*, 1985] and water depth 120 m shallower. The S1 headwall measures only 20–30 m high, but the Chirp data indicate a vertical distance of ~60 m from the top of the headwall to the slide rupture surface. Thus the S1 rupture surface may have intersected the base of gas hydrate stability calculated for the last sea level lowstand (Figure 3b). However, slides associated with the other scarps, which are all located at greater water depths, probably are not directly connected to gas hydrates phase boundary: The base of the gas hydrate stability zone would have lain well below the S2 to S5 slide headwalls and interpreted rupture surfaces at the time of the last sea level lowstand (Figure 6).

4.2.2. Salt Tectonics

[20] One of the most striking observations at the CFS is the location of slide headwalls directly upslope from the breached Cape Fear diapir (Figure 2). While the possible connection between salt diapirism and formation of the CFS has previously been discussed by *Popenoe et al.* [1993], most studies linking salt mobilization and slide triggering have been carried out for salt tectonics provinces like the Gulf of Mexico. In such settings, buried buoyant salt is believed to intrude denser, overlying sediments, leading to active fracturing and slope oversteepening, formation of faults directly above the rising diapir, and eventually slope failure along oversteepened diapiric flanks [*Cashman and Popenoe*, 1985]. In this scenario, salt diapirism is regarded as the *trigger* for faulting above salt domes and associated slope failures.

[21] At the CFS site, the interaction of the slide with salt diapirs seems to be slightly different. Our new data reveal a previously unrecognized normal fault scarp that runs south from the main S4 CFS headwall toward the Blake Ridge Diapir (Figures 2 and 5). In addition, both the new Chirp data and older single channel seismic data collected land-
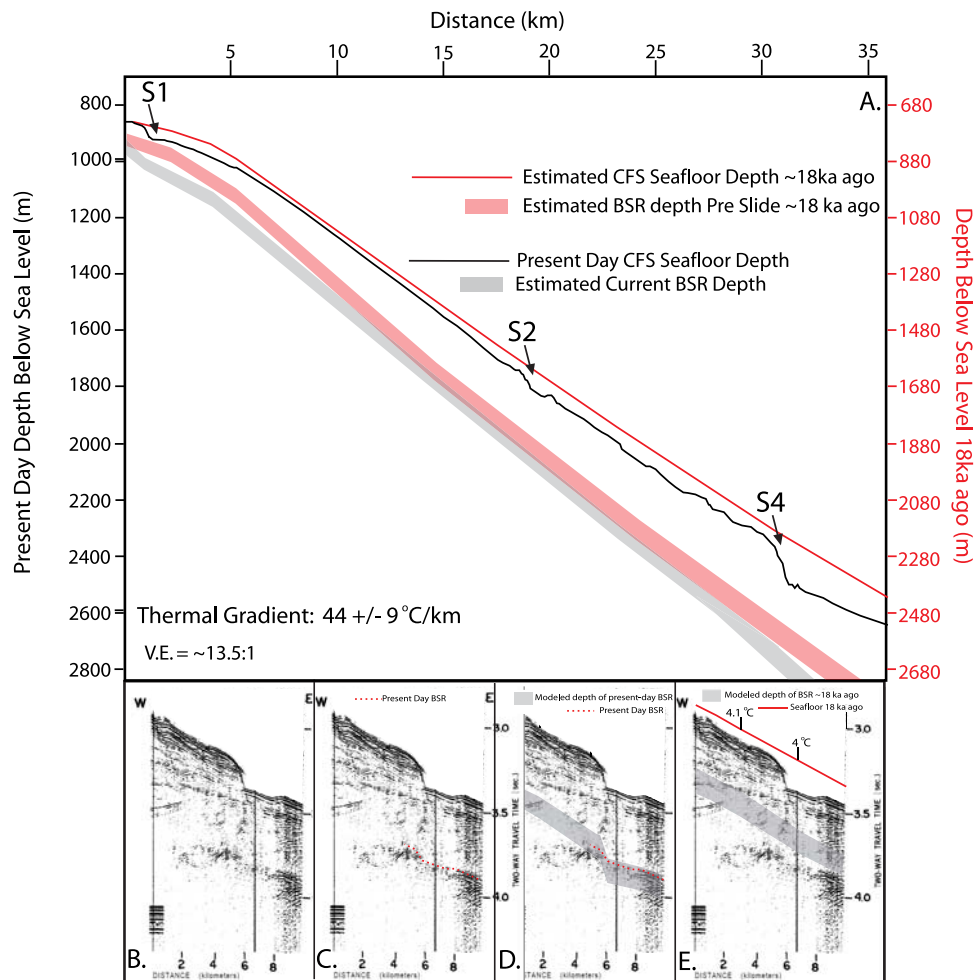
Figure 6. Figure 6a is a cross section of the Cape Fear Slide showing the predicted seafloor depth during the last sea level lowstand (assumed ~18 ka ago, red line) and the estimated gas hydrate phase boundary (pink area), compared with the current seafloor depth (black line) and current gas hydrate phase boundary depth (gray area). Note that the pink area only approaches the black line and slide rupture surface at the shallowest slide site (S1), indicating that the phase boundary was likely too deep to be directly involved in the initiation of the slides associated with scarps S2 through S5. Figures 6b–6e show a regional seismic line collected across the S4 slide by *Dillon et al.* [1982]. The raw seismic data are shown in Figure 6b, with the present-day BSR depth marked as a red dashed line in Figure 6c. In Figure 6d we show the modeled depth of the present-day BSR, with the uncertainty bounds related to both the bottom water temperature and geothermal gradient. The model accurately predicts the present-day BSR depth. Figure 6e shows the calculated location of the BSR and seafloor at 18 ka. The gas hydrate stability conditions were determined using bottom water temperatures of 4.1°C and 4°C at the locations marked in the diagram. At 18 ka the phase boundary was shallower than today but did not intersect the base of the headwall.

ward of the slide suggest that all of the CFS events occurred above an actively deforming graben [*Dillon et al.*, 1982]. These observations are consistent with the inference that regional extensional tectonics, rather than salt mobilization alone, may control the ultimate configuration of salt in the area and play a critical role in slide triggering. Studies in other provinces affected by salt tectonics show that regional extension often governs the location, orientation, and even size of subsurface salt bodies;

that faults and grabens predate salt diapirs instead of these features developing to accommodate rising salt; and that overburden density may be lower than that of buried salt in some places, eliminating buoyancy as a diapiric agent [*Hudec and Jackson*, 2002; *Jackson and Vendeville*, 1994]. Therefore it is possible that salt diapirism along the mid-Atlantic Margin is at least partially "reactive" [*Jackson and Vendeville*, 1994], meaning that salt flows up along faults only as long as extension occurs.

[22] The coincidence of normal faulting, a buried graben, and salt diapirism at the CFS leads us to propose a scenario conducive for slope failure in this area. The new multibeam bathymetric data reveal that the newly recognized normal fault intersects the south side of the main CFS headwall (S4). In the bathymetric data, the scarp of the east-dipping normal fault can be traced from the Blake Ridge Diapir to nearly the breached Cape Fear Diapir. The Cape Fear Diapir lies along the strike of the projected fault about 10 km northeast of the intersection of the fault with the S4 headwall, where the fault's trace is lost beneath slide rubble.

[23] From the Chirp and bathymetric data, we infer different degrees of interaction among the normal fault, buried salt, and seafloor sediment along three cross-sections oriented roughly east-west between the Blake Ridge Diapir on the south and the Cape Fear Diapir on the north. Although the cross-sections were chosen to represent specific locations across the outer shelf break, they also provide a means for assessing the interaction of tectonic and seafloor surface processes with time. Initially, extensional processes caused the formation of the east-dipping normal fault and the upward flow of salt along the footwall. In the hanging wall, the seafloor gradually steepened and likely became the locus for thicker sediment accumulations, eventually producing minor slope failure and slumping (Figure 7b). This situation probably best describes the current state at the position of Profile bb', the most southerly of the three cross-sections. Salt continued to rise with continuing displacement on the normal fault, in turn leading to more slumping in the hanging wall and more displacement on the fault as salt was removed. This intermediate stage in the evolution of the CFS area is probably best represented by Profile cc' (Figure 7c). At the location of the CFS and Profile dd' (Figure 7d), the system has reached maturity, but could still experience future slope failures: Salt movement has progressed to the point that salt pierces the seafloor. During the rise of the salt, the hanging wall slope likely oversteepened while also accumulating thick sediment behind the diapiric backstop. A combination of factors, including the thick
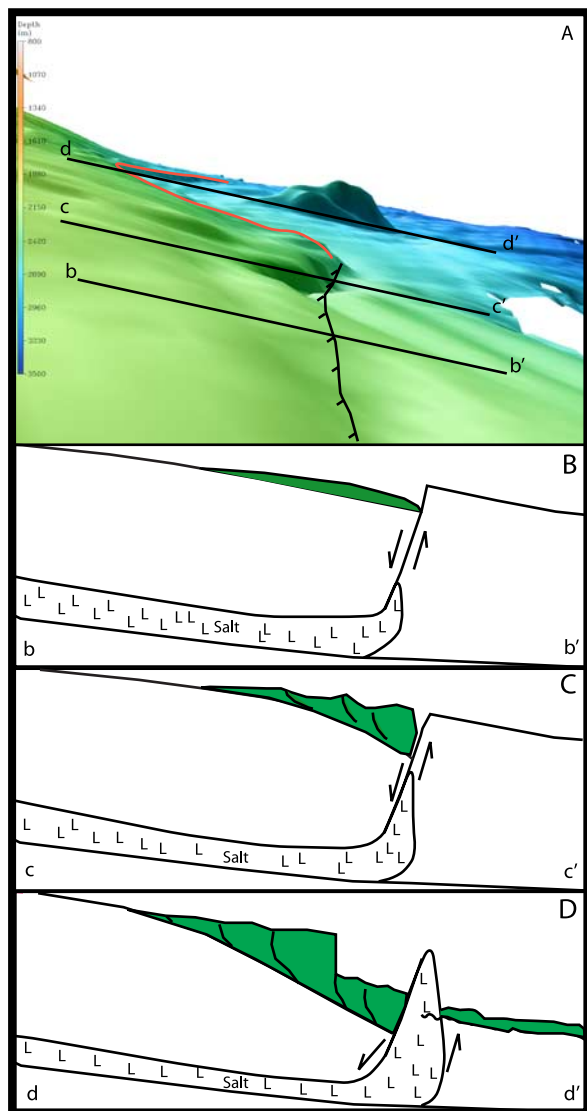
Figure 7. A schematic model describing how normal faulting and reactive salt tectonics may cause sliding. (a) Three-dimensional view of the CFS from the south, assuming a vantage point near the Blake Ridge Diapir and looking along the strike of the normal fault (black line with tick marks). The red line denotes the location of the S4 headwall, and the solid black lines show the locations of interpreted cross sections bb', cc', and dd' (Figures 7b, 7c, and 7d, respectively). Although Figures 7b through 7d correspond to different parts of the fault, they also serve as a proxy for the impact of salt migration along the normal fault over time: The northernmost profile (dd') captures the most advanced stage of salt intrusion, and the southernmost profile captures the least (bb'). (B) Cross section coincident with CFS line 59, where the normal fault is observed. This likely represents the configuration of slumps (green), salt (hatched), and the normal fault at the CFS before sliding initiated. (C) As normal faulting progressed, salt began to evacuate the subsurface, resulting in slope steepening along the down-dropped portion of the fault and some sliding. (D) Continued salt extrusion resulted in even further steepening, perpetuating mass wasting at the site and eventually leading to breaching of the salt structure.
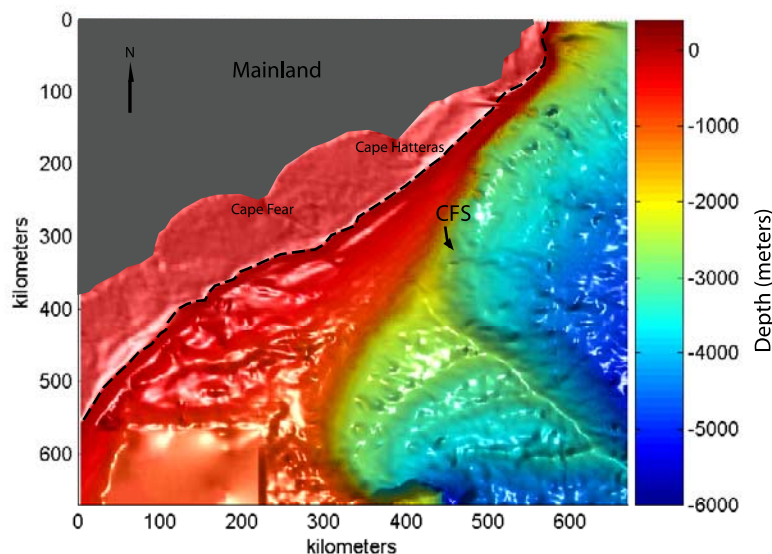
Figure 8. Bathymetric map of the slide/tsunami model domain using the ETOPO2v2 2-min grid. The dashed black line shows the approximate location of the 100 m contour.

and rapid (50–250 m/Ma) accumulation of fine-grained sediment and seafloor oversteepening due to extension and salt withdrawal, probably contributed to slope failure in the CFS area [*Paull et al.*, 1996b].

[24] This scenario for the evolution of the CFS and the outer shelf break south to the Blake Ridge Diapir requires active extrusion of salt along a normal fault. Yet, there is little evidence for significant teleseismic activity along this margin. Nonetheless, shallow low-magnitude earthquakes are periodically recorded along the US margin [*Ekström*, 2006], perhaps suggesting that thin-skinned tectonic deformation may be minor, but ongoing.

4.3. Tsunamogenic Potential of the Cape Fear Slide

4.3.1. Model Formulation

[25] The size of tsunami generated by submarine slides depends on modeling technique and several slide-related parameters, including shape, size, density, displacement, acceleration, velocity, depth, and travel time; however, to first order, slide size, water depth, and velocity profile define tsunami wave height [*Fine et al.*, 2005; *Grilli and Watts*, 1999, 2005; *Jiang and LeBlond*, 1992, 1993; *Matsuyama et al.*, 1999; *Murty*, 2003; *ten Brink et al.*, 2006; *Ward*, 2001]. Without substantial

constraints on these parameters, evaluating the tsunamogenic potential of submarine slides is difficult. The new data and interpretations presented here reduce the uncertainties on several parameters, including the approximate depth, shape, and size of the CFS events. Here, we investigate preliminary slide and tsunami models for the S1 and S4 CFS events.

[26] To first order, the initial shape and kinematics of a slide determine tsunami wave characteristics [*Jiang and LeBlond*, 1992; *Watts et al.*, 2005]. We therefore adopt a one-way coupled wave model in which we first estimate slide motion and then use these results to calculate the resulting waves generated at the sea surface based on the shallow water wave approximation. Changes in slide shape due to dispersion during slide evolution exercise only a secondary effect on the tsunami waves and are therefore ignored in this model [*Watts*, 1997]. The model domain covers an area of ~450,000 km² (670 × 670 km), with square cells that are 230 m on a side. For bathymetry, we interpolated ETOPO2v2 2-min, satellite-based bathymetry onto the 230 m grid and use a Mercator projection (Figure 8).

[27] The new multibeam bathymetric data allow us to estimate the general shape and size of the initial slide source areas for the S1 and S4 slides. The crown-shaped S1 and S4 slide escarpments suggest that, to first order, a scallop-shaped debris flow initially moved down slope. To approximate the

Table 1. Variables and Adopted Values for Submarine Slide and Tsunami Models

Variable	Physical Meaning	Value Assigned
θ	slide slope angle	3°
C_m	mass density coefficient	1
C_n	basal Coulomb coefficient	0.32
C_d	drag coefficient	2
B	characteristic length of slide	10 km
γ	relative density = density of slide/density of water	1.7

shape of the slide, we assume a three-dimensional (3-D) Gaussian beam that matches slide dimensions. Such an assumption has been adopted in a range of previously published slide and tsunami studies, represents a reasonable approximation to the shape of observed and modeled slides, and ensures stability for the coupled surface wave tsunami model [*Grilli and Watts*, 2005; *Jiang and LeBlond*, 1993; *Prior et al.*, 1979; *Watts*, 1997; *Watts et al.*, 2005].

[28] From the new data, we determine that the upper slide (S1) has a headwall height of ∼20 m, ∼60 m above the rupture surface, and a crown scarp diameter of ∼10 km. The initial slide shape is therefore approximated as a 3-D Gaussian with a diameter of ∼10 km (1σ) and a maximum height of 20 m above the surrounding seafloor, with the peak of the Gaussian placed at 890 mbsl. Similarly, the main CFS headwall (S4), which is located at 2300 m water depth, has a maximum height of ∼120 m, a width of ∼50 km, and maximum length from headwall to the salt diapir of ∼10 km. We therefore define the initial slide shape as a Gaussian with a maximum height of 120 m, a width of ∼50 km (1σ), and a length of ∼10 km (1σ).

[29] The displacement S of the slide's center of mass as a function of time t is given by

$$(\gamma + C_m)\frac{d^2S}{dt^2} = (\gamma - 1)(\sin\theta - C_n\cos\theta)g - C_d\frac{2}{\pi B}\left(\frac{dS}{dt}\right)^2, \quad (1)$$

where other variables are as given in Table 1 [*Grilli and Watts*, 2005; *Watts*, 1997; *Watts et al.*, 2005]. Of all these variables, the initial downslope length B of the slide source area remains the most difficult to constrain. Although the width of the flow can be bracketed based on observations of headwall width, the slide's initial length is difficult to determine, particularly since slides (unlike consolidated slumps) often do not create clearly

distinguishable slide blocks that can be used to determine slide area. For both the S1 and S4 slides, we adopted a slide length of 10 km. In the case of S1, this slide length is probably conservative since the slide may have extended at least several kilometers more downslope. For the S4 event, 10 km represents the distance between the headwall and the diapir, which is also the greatest extent to which we can clearly trace the headwall (Figure 2). In general, the greater the slide source length, the larger the volume of slide material, resulting in more displaced water and a potentially larger tsunami.

[30] Higher slide velocities and accelerations produce larger tsunamis [*Harbitz*, 1992; *Tinti et al.*, 2001; *Ward*, 2001], and therefore robust estimates of slide kinematics are required to accurately predict tsunami wave height. To determine velocity and acceleration, we initially adopt the method of *Watts* [1997] and *Grilli and Watts* [1999, 2005]. On the basis of their assumptions, an analytical solution to (1) for velocity $v = dS/dt$ is

$$v(t) = u_t \tanh\left[\frac{a_0 t}{u_t}\right], \quad (2)$$

where u_t is the terminal velocity of the slide, and a_0 denotes the initial slide acceleration, which is calculated from $a_0 = g(\gamma - 1)/(\gamma - C_m)\sin\theta$. For the CFS, we estimate $\gamma = 2$, $\theta \approx 3°$, and $C_m = 1$ (Table 1).

[31] Although we can use (2) to directly calculate the terminal velocity by adopting assumptions about the drag coefficients, and slide shape, size, density, and slope angle, [*Grilli and Watts*, 1999], these parameters may change significantly as the slide progresses. Another key difficulty with determining terminal velocity is its dependence on initial slide length [*Grilli and Watts*, 1999]. For example, we obtain terminal velocity of ∼90 m s^{-1} for S1 for a 10-km-long slide but ∼30 m s^{-1} for a 1-km-long slide. Indirect measurements of slide velocities based on the timing of slide-associated submarine cable breaks suggest velocities of 6 m s^{-1} to more than 30 m s^{-1} for slides consisting of low-density hemipelagic mud [*Bjerrum*, 1971; *Heezen and Ewing*, 1952; *Heezen and Drake*, 1964; *Krause et al.*, 1970]. Therefore we apply an upper limit of 30 m s^{-1} for the terminal velocities of all modeled mudslides.

[32] The water wave created by the mudslide is modeled using the nonlinear shallow-water wave approximation, which constrains wave propagation

characteristics based on two-dimensional continuity and momentum constraints. A similar approach has been adopted in other published tsunami models [e.g., *Fine et al.*, 2005; *Heinrich et al.*, 2000]. One minor improvement we have incorporated here is the inclusion of the Coriolis force in the momentum formulation.

[33] The shallow water wave approximation assumes that wave displacement occurs only in the vertical direction and is small relative to wavelength, meaning that pressures remain hydrostatic. This assumption simplifies the Navier-Stokes equations and reduces the time and complexity of tsunami numerical simulation. Tsunami in deep water typically have small (<1 m) amplitudes compared to their large (>1 km) wavelengths, rendering the shallow water wave approximation appropriate. The assumption breaks down in shallow, nearshore regions, where wavelengths shorten, wave heights approach ocean depths, and both the hydrostatic approximation and the assumption of vertical-only wave displacement become invalid. Like many other published tsunami models, our model yields a robust first-order prediction of near-field wave formation and amplitude in deep water and of the propagation pattern of the wave toward the coast. For this study, the amplitude of the sea surface wave at the 100 m bathymetric contour provides a useful metric for evaluating the potential of the tsunami to have a significant impact on coastal areas as they approach the shoreline.

4.3.2. Tsunami Model Results and Implications

[34] Analysis of model results shows that the S1 slide likely produced a small tsunami, but that the S4 slide produced a potentially hazardous event. The maximum sea surface wave height produced by the S1 slide event at the present-day 100 m bathymetric contour off the U.S. Eastern Seaboard is 0.68 m. As a comparison, tsunami models for the 1929 Grand Banks Slide, the Storegga Slide, and the 1998 Papua New Guinea slide, as well as other slides along the U.S. mid-Atlantic margin, all predict maximum sea surface waves of at least a meter at this bathymetric contour [*Harbitz*, 1992; *Heinrich et al.*, 2000; *Ward*, 2001; *Ward and Day*, 2005]. We therefore infer that the S1 CFS event did not produce a significant tsunami.

[35] In contrast, results for the S4 slide show that this event produced significantly larger sea surface waves than the S1 slide. The amplitude of the near-field sea surface wave exceeds 2 m at the present-

day 100 m bathymetric contour (Figure 9b). Although the S4 tsunami would be expected to increase in amplitude as the waves approached shore, dispersion through frictional forces should temper such wave growth. Nonetheless, even a 2-m-high wave would inundate a significant portion of the low-lying Carolina coast and barrier islands. The modeled wave height exceeds 2 m for a 50 km stretch along the 100 m contour, indicating that tens of kilometers of coastline could be affected by the near-field wave. The model shows that the tsunami initially makes landfall near Cape Hatteras, North Carolina, with the wave taking approximately 1.5 hr to reach shore from the time of slide initiation. Assuming that the S4 occurred during the last sea level low-stand, no evidence of this event should exist along the present-day coastline because the paleoshoreline would have been located near the present-day ∼120 m bathymetric contour.

4.3.3. Assessing the Potential for Future Slides and Tsunami

[36] In light of the past repetitive nature of slide events at the CFS and the possibility that some CFS events might have been associated with significant tsunami, a key question is whether similar slides and tsunami could occur in the future. The relatively poor constraints on slide timing and triggering mechanisms and the volume of material mobilized in each slide render it difficult to fully address this issue. Other parts of the North American Atlantic margin have also experienced persistent and periodic slide events, and further slope failures at the CFS might be expected if this area fits the larger regional pattern. The graben beneath the CFS complex remains active [*Dillon et al.*, 1982], meaning that continuing salt intrusion associated with ongoing normal fault displacement might lead to new slope steepening and the triggering of new slides. Nonetheless, good evidence exists that overpressures associated with sediment loading during sea level low-stand may be the most important facilitator for slide initiation [*Dugan and Flemings*, 2002], and that salt intrusion, faulting and gas hydrate may have less impact on slope stability.

[37] Although gas hydrate dissociation may act as a slide triggering mechanism in water depths between 500–1000 m, our analysis indicates that the evidence for slide failure along a critically pressured gas-hydrate phase boundary, for all but the shallowest CFS events, is tenuous at best. In the future, warming oceans would lead to the dissoci-
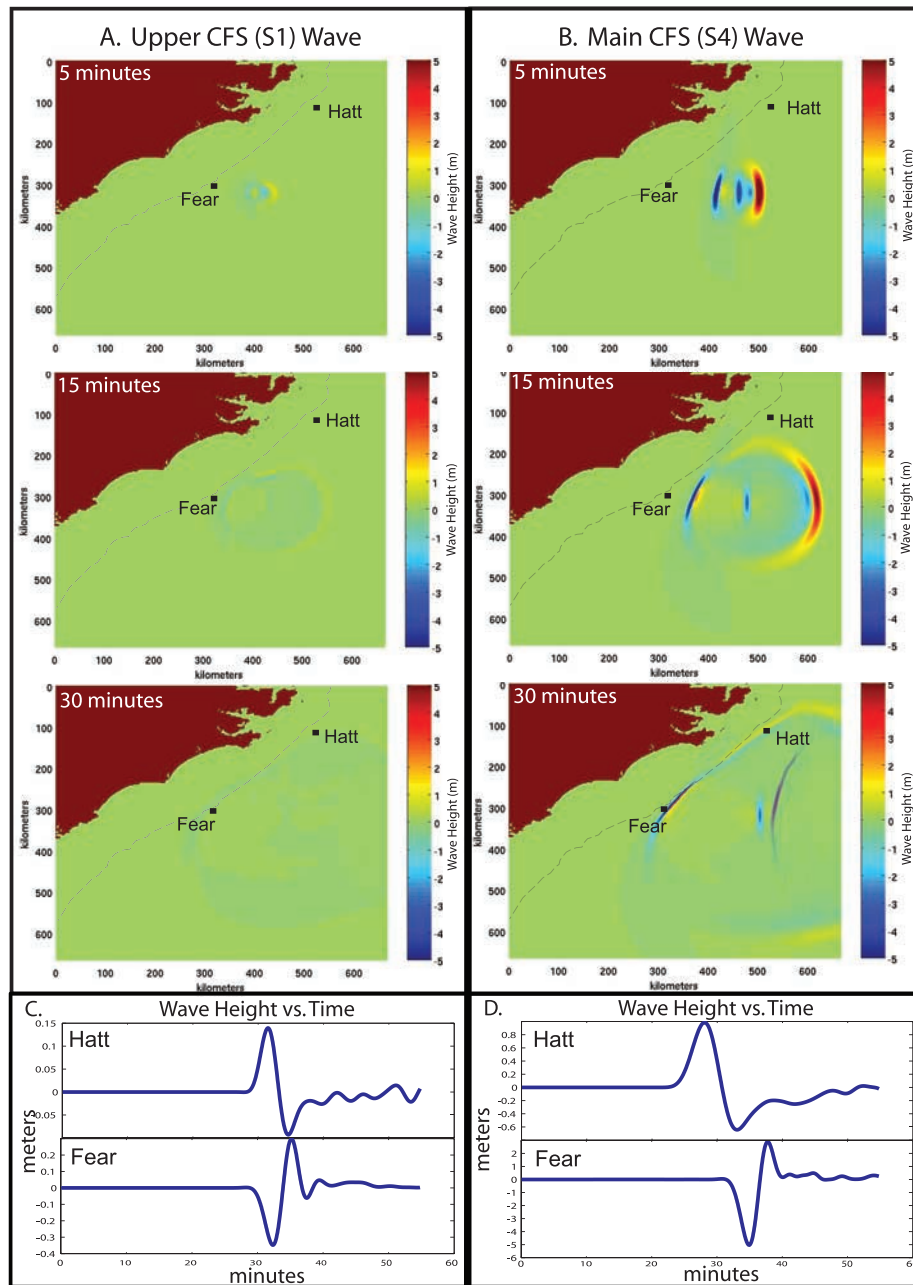
Figure 9. Map view showing wave model results for 5, 15, and 30 min after slide initiation of the S1 CFS (Figure 9a) and the S4 CFS (Figure 9b) and the change in sea level over time created at hypothetical buoys "Hatt" (for Cape Hatteras) and "Fear" (for Cape Fear) by each slide (Figures 9c and 9d). Dashed gray lines indicate the approximate location of the 100 m contour. As shown in Figures 9a and 9c, the sea surface amplitudes generated by the S1 slide are significantly less than those for the S4 slide (Figures 9b and 9d). Thirty minutes after initiation of sliding for the S1 event, sea surface waves less than 1 m high cross the 100 m contour. As shown in Figures 9b and 9d, a sea surface wave of total amplitude ~8 m approaches the 100 m contour at the Fear buoy ~30 min after sliding begins for the S4 event, with a ~1 m wave approaching the Hatt buoy. These amplitudes may increase as the wave approaches shore, but slower wave speeds over the extensive western Atlantic shelf will promote viscous wave dampening and dispersion.

ation of some of the present-day gas hydrate deposits, thereby increasing pressures in sediments if gas is produced, but does not escape. Offsetting the impact of warmer temperatures on the present-

day gas hydrate reservoir is the increased pressure associated with sea level rise. Though pressure changes on the gas hydrate reservoir are more instantaneous than temperature changes, which

propagate downward at a rate determined by the sediment's thermal diffusivity [*Ruppel*, 2000], the destabilizing impact of ocean warming is eventually expected to outpace the stabilizing effect of pressure increases.

5. Conclusions

[38] The outer shelf break in the Cape Fear area has been the site of a series of complex slides, and new bathymetric data reveal at least five separate events based on the identification of exposed headwalls. Buried headwalls imaged beneath the slide deposits with new Chirp data indicate that even more slides may have occurred at the site. Within the context of slides arrayed along nearly the entire length of the North American Atlantic margin, the CFS complex is probably not unusual. With the discovery that the CFS consists of at least five separate slides that have been triggered within the past ∼30ka, we suggest that slides along the margin may occur with perhaps significantly higher frequency than previous studies indicate.

[39] Although the exact trigger mechanism for Cape Fear slide events remains poorly constrained, our analysis offers new insight into the role that methane gas and regional tectonics play in slope stability. Specifically, we suggest that, for all but the shallowest event, sliding occurred well above the gas hydrate phase boundary. Similar results have recently been obtained for the massive Storegga Slide, which was previously linked to gas hydrate triggering as well [*Brown et al.*, 2006]. Therefore gas hydrate phase boundaries may not necessarily act as the primary slide rupture surface. To resolve the role that gas hydrates play in slope failure requires significantly improved age constraints and better controls on ocean temperature, regional geotherms, and sedimentary pressure conditions when these slides occurred. A more detailed analysis linking hydrate dissociation, pore pressure, and shear strength with ocean temperature/pressure models will ultimately improve our understanding of hydrate as a potential slope failure trigger.

[40] Down-drop along a normal fault that runs from the Cape Fear Diapir on the northeast to the Blake Ridge Diapir on the southwest and that intersects the main CFS headwall may have caused slope steepening that contributed to sliding in this area. This fault, visible in seafloor bathymetric data, appears active, and displacement associated with further extension could trigger future slides

and tsunami in the region. Initial results from first-approach slide/tsunami models for the CFS complex indicate that some past slide events produced large enough tsunami to be considered a potential geohazard. More detailed constraints on slide size and dynamics could substantially improve our understanding of both the CFS and resulting tsunami.

Acknowledgments

References

Bea, R. G., S. G. Wright, P. Sicar, and A. W. Niedoroda (1983), Wave-induced slides in South Pass Block 70, Mississippi delta, *J. Geotech. Eng.*, *109*, 619–644.

Bjerrum, L. (1971), Subaqueous slope failures in Norwegian fjords, *Norw. Geotech. Inst. Bull.*, *88*, 1–8.

Booth, J. S., D. W. O'Leary, P. Popenoe, and W. W. Danforth (1993), Atlantic continental slope landslides: Their distribution, general attributes, and implications, in *Submarine Landslides: Selected Studies in the U.S. Exclusive Economic Zone*, edited by W. C. Schwab, H. J. Lee, and D. C. Twichell, *U.S. Geol. Surv. Bull. 2002*, 14–22.

Brown, H. E., W. S. Holbrook, M. J. Hornbach, and J. Nealon (2006), Slide structure and role of gas hydrate at the northern boundary of the Storegga Slide, offshore Norway, *Mar. Geol.*, *229*(3–4), 179–186.

Caress, D. W., and D. N. Chayes (1995), New software for processing sidescan data from sidescan-capable multibeam sonars, in *Oceans '95: Challenges of Our Changing Global Environment*, pp. 997–1000, Inst. of Electr. and Electron. Eng., New York.

Carpenter, G. (1981), Coincident sediment slump/clathrate complexes on the US Atlantic continental slope, *Geo Mar. Lett.*, *1*, 29–32.

Cashman, K. V., and P. Popenoe (1985), Slumping and shallow faulting related to the presence of salt on the Continental Slope and Rise off North Carolina, *Mar. Pet. Geol.*, *2*, 260–271.

Crozier, M. J. (1984), Field assessment of slope instability, in *Slope Instability*, edited by D. Brunsden and D. B. Prior, pp. 103–142, John Wiley, New York.

Dillon, W. P., and P. Popenoe (1988), The Blake Plateau Basin and Carolina Trough, in *The Atlantic Continental Margin, U.S. V.I-2 of the Geology of North America*, edited by R. E. Sheridan and J. A. Grow, pp. 291–328, Geol. Soc. of Am., Boulder, Colo.

Dillon, W. P., P. Popenoe, J. A. Grow, K. D. Klitgord, B. A. Swift, C. K. Paull, and K. V. Cashman (1982), Growth faulting and salt diapirism: Their relationship and control in the Carolina Trough, eastern North America, in *Studies of Continental Margin Geology*, edited by J. S. Watkins and C. L. Drake, *AAPG Mem.*, *34*, 21–46.

Driscoll, N. W., J. K. Weissel, and J. A. Goff (2000), Potential for large-scale submarine slope failure and tsunami generation along the U.S. mid-Atlantic coast, *Geology*, *28*(5), 407–410.

Dugan, B., and P. B. Flemings (2000), Overpressure and fluid flow in the New Jersey continental slope: Implications for slope failure and cold seeps, *Science*, *289*, 288–291.

Dugan, B., and P. B. Flemings (2002), Fluid flow and stability of the US continental slope offshore New Jersey from the Pleistocene to the present, *Geofluids*, *2*, 137–146.

Ekström, G. (2006), Global detection and location of seismic sources by using surface waves, *Bull. Seismol. Soc. Am.*, *96*(4A), 1201–1212.

Embley, R. M. (1980), The role of mass transport in the distribution and character of deep-ocean sediments with special reference to the North Atlantic, *Mar. Geol.*, *38*, 25–50.

Embley, R. M., and R. D. Jacobi (1986), Mass wasting in the western North Atlantic, in *The Western North Atlantic Region*, edited by P. R. Vogt and B. E. Tucholke, pp. 479–490, Geol. Soc. of Am., Boulder, Colo.

Fine, I. V., A. B. Rabinovich, B. D. Bornhold, R. E. Thomson, and E. A. Kulikov (2005), The Grand Banks landslide-generated tsunami of November 18, 1929: Preliminary analysis and numerical modeling, *Mar. Geol.*, *215*, 45–57.

Flemings, P. B., X. L. Liu, and W. J. Winters (2003), Critical pressure and multiphase flow in Blake Ridge gas hydrates, *Geology*, *31*(12), 1057–1060.

Grilli, S. T., and P. Watts (1999), Modeling of waves generated by a moving submerged body: Applications to underwater landslides, *Eng. Anal. Boundary Elem.*, *23*, 645–656.

Grilli, S. T., and P. Watts (2005), Tsunami generation by submarine mass failure. I: Modeling, experimental validation, and sensitivity analysis, *J. Waterw. Port Coastal Ocean Eng.*, *131*, 283–297.

Hampton, M. A., H. J. Lee, and J. Locat (1996), Submarine slides, *Rev. Geophys.*, *34*(1), 33–59.

Harbitz, C. B. (1992), Model simulations of tsunamis generated by the Storegga Slides, *Mar. Geol.*, *105*, 1–21.

Heezen, B. C., and C. L. Drake (1964), Gand Banks Slump, *Am. Assoc. Pet. Geol. Bull.*, *48*(2), 221–233.

Heezen, B. C., and M. Ewing (1952), Turbidity currents and submarine slumps, and the 1929 Grand Banks earthquake, *Am. J. Sci.*, *250*, 849–873.

Heinrich, P., A. Piatanesi, E. Okal, and H. Heberte (2000), Near-field modeling of the July 17, 1998 tsunami in Papua New Guinea, *Geophys. Res. Lett.*, *27*(19), 3037–3040.

Henkart, P. (2006), SIOSEIS, Scripps Inst. of Oceanogr., Univ. of San Diego, San Diego, Calif.

Hornbach, M. J., D. M. Saffer, and W. S. Holbrook (2004), Critically pressured free-gas reservoirs below gas-hydrate provinces, *Nature*, *427*(6970), 142–144.

Hudec, M. R., and M. P. A. Jackson (2002), Structural segmentation, inversion, and salt tectonics on a passive margin: Evolution of the Inner Kwanza Basin, Angola, *Geol. Soc. Am. Bull.*, *114*(10), 1222–1244.

Jackson, M. P. A., and B. C. Vendeville (1994), Regional extension as a geologic trigger for diapirism, *Geol. Soc. Am. Bull.*, *106*(1), 57–73.

Jiang, L., and P. H. LeBlond (1992), The coupling of a submarine slide and the surface wave which it generates, *J. Geophys. Res.*, *97*(C8), 12,731–12,744.

Jiang, L., and P. H. LeBlond (1993), Numerical modeling of an underwater Bingham plastic mudslide and the wave which it generates, *J. Geophys. Res.*, *98*(C6), 10,303–10,319.

Kayen, R. E., and H. J. Lee (1993), Slope stability in regions of sea-floor gas hydrate: Beaufort Sea continental slope, in *Submarine Landslides: Selected Studies in the U.S. Exclusive Economic Zone*, edited by W. C. Schwab, H. J. Lee, and D. C. Twichell, *U.S. Geol. Surv. Bull. 2002*, 97–103.

Krause, D. C., W. C. White, D. J. W. Piper, and B. C. Heezen (1970), Turbidity currents and cable breaks in the western New Britain Trench, *Geol. Soc. Am. Bull.*, *81*, 2153–2160.

Locat, J., and H. J. Lee (2002), Submarine landslides: Advances and challenges, *Can. Geotech. J.*, *39*(1), 193–212.

Maslin, M., N. Mikkelsen, C. Vilela, and B. Haq (1998), Sea-level- and gas-hydrate-controlled catastrophic sediment failures of the Amazon Fan, *Geology*, *26*(12), 1107–1110.

Maslin, M., M. Owen, S. Day, and D. Long (2004), Linking continental-slope failures and climate change: Testing the clathrate gun hypothesis, *Geology*, *32*(1), 53–56.

Maslin, M., C. Vilela, N. Mikkelsen, and P. Grootes (2005), Causes of catastrophic sediment failures of the Amazon Fan, *Quat. Sci. Rev.*, *24*(20–21), 2180–2193.

Matsuyama, M., J. P. Walsh, and H. Yeh (1999), The effect of bathymetry on tsunami characteristics at Sisano Lagoon, Papua New Guinea, *Geophys. Res. Lett.*, *26*(23), 3513–3516.

Mienert, J., M. Vanneste, S. Bunz, K. Andreassen, H. Haflidason, and H. P. Sejrup (2005), Ocean warming and gas hydrate stability on the mid-Norwegian margin at the Storegga Slide, *Mar. Pet. Geol.*, *22*(1–2), 233–244.

Murty, T. S. (2003), Tsunami wave height dependence on landslide volume, *Pure Appl. Geophys.*, *160*(10–11), 2147–2153.

O'Leary, D. W., and M. R. Dobson (1992), Southeastern New England continental rise: Origin and history of slide complexes, in *Geological Evolution of Atlantic Continental Rises*, edited by C. W. Poag and P. C. de Graciansky, pp. 214–265, Van Nostrand Reinhold, New York.

Paull, C. K., W. J. Buelow, W. Ussler, and W. S. Borowski (1996a), Increased continental-margin slumping frequency during sea-level lowstands above gas hydrate-bearing sediments, *Geology*, *24*(2), 143–146.

Paull, C. K., et al. (Eds.) (1996b), *Proceedings of the Ocean Drilling Program, Initial Reports*, vol. 164, 623 pp., Ocean Drill. Program, College Station, Tex.

Paull, C. K., P. G. Brewer, W. Ussler, E. T. Peltzer, G. Rehder, and D. Clague (2003), An experiment demonstrating that marine slumping is a mechanism to transfer methane from seafloor gas-hydrate deposits into the upper ocean and atmosphere, *Geo Mar. Lett.*, *22*(4), 198–203.

Pecher, I. A., S. A. Henrys, S. Ellis, S. M. Chiswell, and N. Kukowski (2005), Erosion of the seafloor at the top of the gas hydrate stability zone on the Hikurangi Margin, New Zealand, *Geophys. Res. Lett.*, *32*, L24603, doi:10.1029/2005GL024687.

Piper, D. J. W., and A. E. Asku (1987), The source and origin of the 1929 Grand Banks turbidity current inferred from sediment budgets, *Geo Mar. Lett.*, *7*, 177–182.

Popenoe, P., E. A. Schmuck, and W. P. Dillon (1993), The Cape Fear landslide: Slope failure associated with salt diapirism and gas hydrate decomposition, in *Submarine Landslides: Selected Studies in the U.S. Exclusive Economic Zone*, edited by W. C. Schwab, H. J. Lee, and D. C. Twichell, *U.S. Geol. Surv. Bull. 2002*, 40–53.

Prior, D. B., J. M. Coleman, and L. E. Garrison (1979), Digitally acquired undistorted side-scan sonar images of submarine landslides, Mississippi River delta, *Geology*, *7*(9), 423–425.

Rodriguez, N. M., and C. K. Paull (2000), Data report: ^{14}C dating of sediments of the uppermost cape fear slide plain: Constraints on the timing of this massive submarine slide, *Proc. Ocean Drill. Program Sci. Results*, *164*, 325–327.

Roemmich, D., and C. Wunsch (1985), Two transatlantic sections: Meridional circulation and heat flux in the subtropical North Atlantic Ocean, *Deep Sea Res., Part A*, *32*(6), 619–664.

Ruppel, C. (2000), Thermal state of the gas hydrate reservoir, in *Natural Gas Hydrate in Oceanic and Permafrost Environments*, edited by M. Max, pp. 29–42, Kluwer Acad., Norwell, Mass.

Ruppel, C., R. P. Von Herzen, and A. Bonneville (1995), Heat flux through an old (∼175 Ma) passive margin: Offshore southeastern United States, *J. Geophys. Res.*, *100*(B10), 20,037–20,058.

Scanlon, K. M. (1982), GLORIA sidescan and seismic data collected by the DESU STARELLA along the continental slope and upper continental rise of the eastern United States in 1979, *U.S. Geol. Surv. Open File Rep.*, *82*(1095), 3 pp.

Schmuck, E. A., and C. K. Paull (1993), Evidence for gas accumulation associated with diapirism and gas hydrates at the head of the Cape Fear Slide, *Geo Mar. Lett.*, *13*(3), 145–152.

Sloan, E. D. (1998), *Clathrate Hydrates of Natural Gas*, 2nd ed., Marcel Dekker, New York.

Solheim, A., K. Berg, C. F. Forsberg, and P. Bryn (2005), The Storrega Slide Complex: Repetitive large scale sliding with similar cause and development, *Mar. Pet. Geol.*, *22*, 97–107.

Sultan, N., et al. (2004a), Triggering mechanisms of slope instability processes and sediment failures on continental margins: A geotechnical approach, *Mar. Geol.*, *213*(1–4), 291–321.

Sultan, N., P. Cochonat, J. P. Foucher, and J. Mienert (2004b), Effect of gas hydrates melting on seafloor slope instability, *Mar. Geol.*, *213*(1–4), 379–401.

ten Brink, U. S., E. L. Geist, and B. D. Andrews (2006), Size distribution of submarine landslides and its implication to tsunami hazard in Puerto Rico, *Geophys. Res. Lett.*, *33*, L11307, doi:10.1029/2006GL026125.

ten Brink, U. S., D. C. Twitchell, E. L. Geist, J. Chaytor, J. Locat, H. J. Lee, B. Buczkowski, and M. Sansourcy (2007), Atlantic and Gulf of Mexico Tsunami Hazard Assessment Group: The current state of knowledge regarding potential tsunami sources affecting U.S. Atlantic and Gulf coasts—A report to the Nuclear Regulatory Commission, Nucl. Regulatory Comm., Washington, D. C.

Tinti, S., E. Bortolucci, and C. Chiavetteri (2001), Tsunami excitation by submarine slide in shallow-water approximation, *Pure Appl. Geophys.*, *158*, 759–797.

Vanneste, M., J. Mienert, and S. Bunz (2006), The Hinlopen Slide: A giant submarine slope failure on the northern Svalbard margin, Arctic Ocean, *Earth Planet. Sci. Lett.*, *245*(1–2), 373–388.

Ward, S. N. (2001), Landslide tsunami, *J. Geophys. Res.*, *106*(6), 11,201–11,215.

Ward, S. N., and S. Day (2005), Tsunami thoughts, in *CSEG Recorder*, pp. 38–44, Can. Soc. of Explor. Geophys., Calgary, Canada.

Watts, P. (1997), Water waves generated by underwater landslides, Calif. Inst. of Technol., Pasadena, Calif.

Watts, P., S. T. Grilli, D. R. Tappin, and G. J. Fryer (2005), Tsunami generation by submarine mass failure. II: Predictive equations and case studies, *J. Waterw. Port Coastal Ocean Eng.*, *131*(6), 298–310.

Wessel, P., and W. H. F. Smith (1991), Free software helps map and display data, *Eos Trans. AGU*, *72*, 445–446.